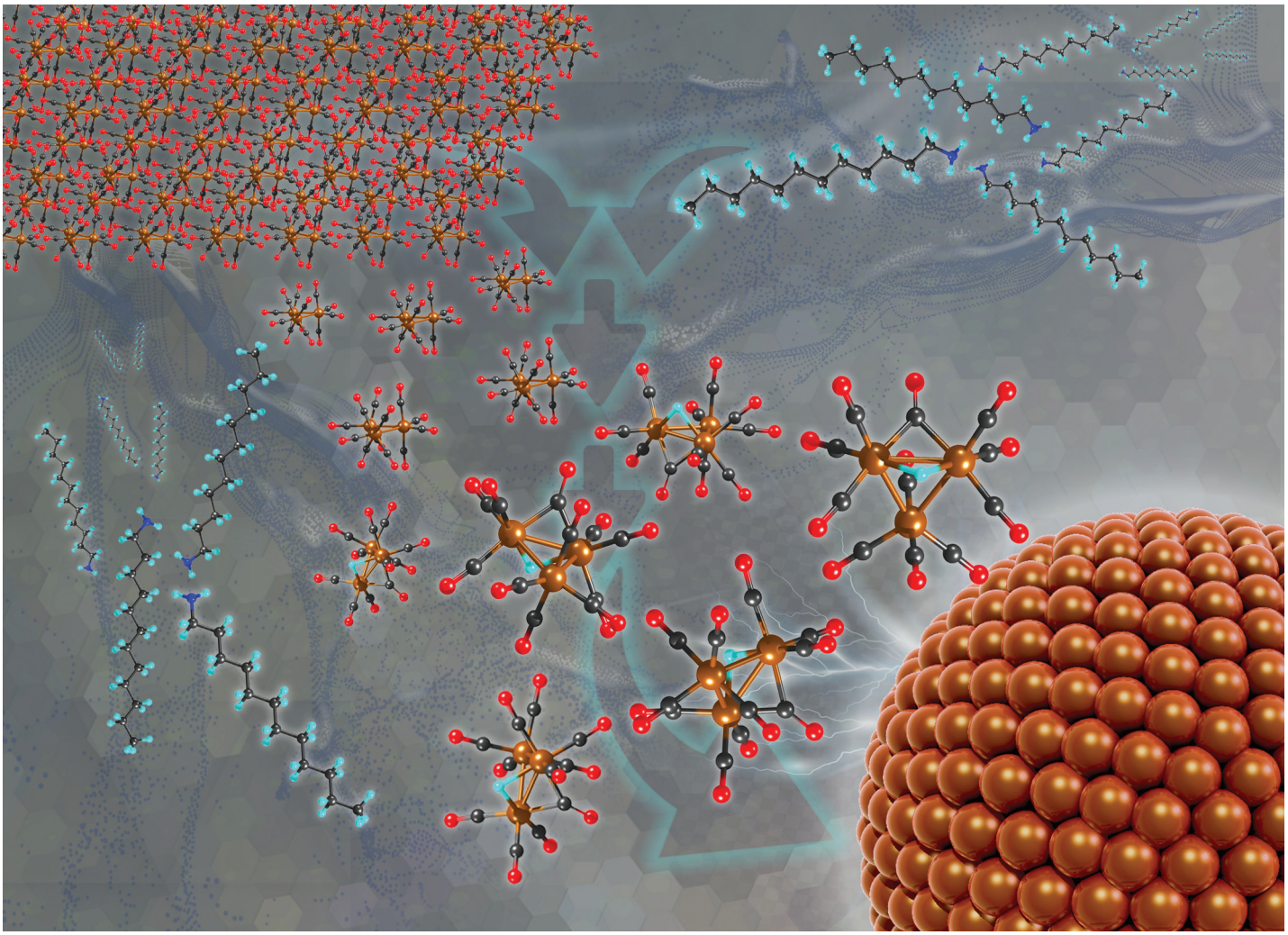

Showcasing research from the Center for Integrated Nanotechnologies at Sandia National Laboratories and Los Alamos National Laboratory.

Non-volatile iron carbonyls as versatile precursors for the synthesis of iron-containing nanoparticles

Iron pentacarbonyl is a popular precursor for the synthesis of iron nanoparticles despite its volatility and toxicity. We demonstrate the formation of a soluble and non-volatile iron precursor by gently heating the insoluble crystalline solid, triiron dodecacarbonyl, in the presence of alkyl amines. We show that this convenient and low-toxicity precursor is a direct replacement for iron pentacarbonyl in the synthesis of a variety of iron-containing nanoparticles.

As featured in:

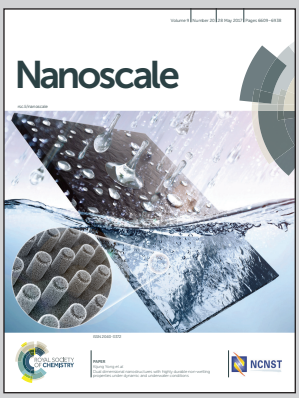

See Dale L. Huber *et al.*, *Nanoscale*, 2017, **9**, 6632.

ROYAL SOCIETY OF CHEMISTRY

rsc.li/nanoscale

Registered charity number: 207890

Nanoscale

COMMUNICATION

View Article Online
View Journal | View Issue

Cite this: *Nanoscale*, 2017, **9**, 6632

Received 12th February 2017,
Accepted 5th March 2017

DOI: 10.1039/c7nr01028a

rsc.li/nanoscale

Non-volatile iron carbonyls as versatile precursors for the synthesis of iron-containing nanoparticles†

John Watt,[a] Grant C. Bleier,[a] Mariah J. Austin,[a] Sergei A. Ivanov[b] and Dale L. Huber*[a]

The most commonly used method for the formation of well-defined iron and iron-containing heterometallic nanoparticles is the thermal decomposition of iron pentacarbonyl ($Fe(CO)_5$). However, iron pentacarbonyl is highly toxic and volatile, which introduces safety concerns and drastically diminishes control over the reaction stoichiometry. Here we alleviate these issues by beginning with an easy-to-handle solid, triiron dodecacarbonyl ($Fe_3(CO)_{12}$). The issue of poor solubility of this cluster is addressed by its reaction with amine, which renders the cluster fully soluble in common high boiling point solvents. This reaction generates non-volatile anionic iron carbonyl species in solution which are subsequently used as the nanoparticle precursor. We demonstrate that the thermolysis of this novel precursor solution yields well-defined Fe, $Fe_{1-x}Co_x$, and $Fe_{1-x}Pt_x$ nanoparticles. In addition, the same approach overcomes the solubility issue of another poorly soluble iron carbonyl compound, diiron nonacarbonyl ($Fe_2(CO)_9$). By using these precursors in an array of nanoparticle-forming reactions, we demonstrate a convenient replacement for the commonly used $Fe(CO)_5$, producing particles of similar quality, but without the drawbacks of the precursor volatility and high toxicity.

Magnetic nanoparticles have enjoyed a large amount of research interest due to their great potential in a range of applications including waste remediation, data storage, and magnetic resonance imaging.[1] Zero-valent iron nanoparticles are particularly attractive due to the high magnetic moment (M_s = 222 Am^2 kg^{-1} @ 273 K) and high susceptibility of bulk iron. Due to low magnetocrystalline anisotropy, iron nanoparticles display superparamagnetic behavior at much larger sizes than other magnetic materials, which makes them excellent candidates for such applications as MRI contrast agents, bioseparation and as recoverable catalysts.[2] Likewise, magnetically soft heterometallic iron-cobalt alloy nanoparticles ($Fe_{1-x}Co_x$) are of significant interest as they possess the highest room temperature saturation magnetization of all known metallic alloys ($M_s \approx 240$ Am^2 kg^{-1} @ 273 K).[3] Iron–platinum ($Fe_{1-x}Pt_x$) nanoparticles, on the other hand, possess a high magnetocrystalline anisotropy ($K \approx 6.6 \times 10^6$ J m^{-3}) and large coercivity (H_c) when annealed to the chemically ordered tetragonal $L1_0$ phase. As such, these nanoparticles have been extensively studied for their potential application in ultra-high density magnetic storage applications and as components in exchange-coupled composite magnets.[4]

Common solution-phase approaches to the synthesis of iron and heterometallic iron-containing nanoparticles include the reduction of iron salts and/or the thermolysis of iron complexes.[4c,5] Perhaps, the most widely used approach is the thermal decomposition of iron pentacarbonyl, $Fe(CO)_5$. This compound is inexpensive and readily available commercially, which makes it a popular choice for nanoparticle synthesis. While $Fe(CO)_5$ has proven valuable for the small-scale research synthesis, its continued use, especially for potential scale up efforts, is severely limited. It is pyrophoric with an auto-ignition temperature of 49 °C and occupational exposure limits are set to an incredibly low 0.1 ppm.[6]

$Fe(CO)_5$ has a low boiling point (103 °C) and under high temperature nanoparticle synthesis conditions unknown quantities can be boiled off, significantly decreasing yield in general and changing iron content in the case of heterometallic particle synthesis. Furthermore, the formation of decomposition products under storage introduces the need for a purification step.[7] It is easy then to see that at larger scales, $Fe(CO)_5$ would present significant technical and safety burdens. The development of a simple, less toxic, and non-volatile precursor that could substitute directly for $Fe(CO)_5$ would be of significant benefit for further synthetic investigations of iron and iron-containing heterometallic nanoparticles.

Here we report the synthesis of well-defined Fe, $Fe_{1-x}Co_x$, and $Fe_{1-x}Pt_x$ nanoparticles from the low-volatility solid and commercially available iron-carbonyl cluster, triiron dodecacarbonyl $Fe_3(CO)_{12}$. $Fe_3(CO)_{12}$ is stable under ambient conditions,

[a]*Sandia National Laboratories, Albuquerque, NM, USA, 87185.*
E-mail: Dale.Huber@sandia.gov
[b]*Los Alamos National Laboratory, Los Alamos, NM, USA, 87545*

†Electronic supplementary information (ESI) available: Full experimental detail, DFT calculations, additional TEM, SAXS, EDX, UV-vis, XRD and FTIR characterization. See DOI: 10.1039/c7nr01028a

easy to handle, and much less toxic than $Fe(CO)_5$.[8] It decomposes at high temperatures, increasing the range of available reaction temperatures, which would allow for improvements in crystallinity.[9] Furthermore, it can be used as received directly from a supplier, removing the need for purification, and thereby simplifying the overall synthetic procedure. The cluster is commonly employed as a catalyst in organic transformations,[10] but it is poorly soluble in high boiling point organic solvents and therefore there are only a few examples of its use as a precursor for nanoparticle synthesis. Shpaisman *et al.* formed nanocrystalline Fe particles by thermally decomposing $Fe_3(CO)_{12}$ under argon flow at high temperatures, and Amara *et al.* formed Fe and Fe_3O_4 nanoparticles by a solvothermal decomposition synthesis.[8,11] Choplin *et al.* formed iron-containing heterometallic particles from carbonyl-containing heteropolynuclear precursor clusters.[12] However, the lack of precursor solubility made size and shape control difficult.

Here, we demonstrate a significant increase in the solubility of $Fe_3(CO)_{12}$ by reacting it with an excess of a long-chain primary alkylamine, 1-dodecylamine (DDA), under an inert atmosphere and mild heating. Multi-metal center iron carbonyl clusters have been reported to form anionic cluster species on surfaces or in amine solvents, usually *via* disproportionation.[13] Here, the formation of such an anionic iron complex leads to the complete dissolution of original $Fe_3(CO)_{12}$ in common solvents employed in nanoparticle synthesis (*e.g.*, 1-octadecene) (ODE), thereby eliminating the multiple synthetic steps that are often required for other complex iron nanoparticle precursors.[3b,14] This easily prepared, non-volatile iron cluster solution is then used here as the actual precursor in thermal decomposition reactions to form well-defined Fe, $Fe_{1-x}Co_x$, and $Fe_{1-x}Pt_x$ nanoparticles, with the DDA as stabilizing agent. The presented approach to the synthesis of iron and iron-containing heterometallic nanoparticles can also be extended to another poorly soluble iron carbonyl cluster, $Fe_2(CO)_9$.

When $Fe_3(CO)_{12}$ is heated in an excess of DDA (1 : 30) under nitrogen (Fig. 1a), a color change from green to deep red is observed indicating the formation of the anionic $[HFe_3(CO)_{11}]^-$ (Fig. 1a).[15] The UV-Vis absorption profile of $Fe_3(CO)_{12}$ in chloroform shows two absorption peaks at 456 and 607 nm, as well as multiple absorption bands stretching into the UV (Fig. 1b). After heating in the presence of excess DDA (Fig. 1c), the strong band at 607 nm blue shifts to 545 nm with a strong second absorption peak now clearly visible at 319 nm, which is consistent with the formation of $[HFe_3(CO)_{11}]^-$. Previously, this deep-red cluster anion has been identified as a disproportionation product of $Fe_3(CO)_{12}$ on the surface of alumina or magnesia.[15] In these studies, $Fe_3(CO)_{12}$ dissociates at a surface and could be liberated by the use of a counteraction, *e.g.*, NEt_4^+. In the present case, the anionic complex forms *in situ* due to the presence of DDA, simplifying the solubilization process. The presence of $[HFe_3(CO)_{11}]^-$ in solution has been confirmed by electrospray ionization mass spectrometry (ESI-MS), revealing the $[HFe_3(CO)_{11}]^-$ (m/z = 476.7) ion (and its decarbonylation products) to be the majority of species present in the precursor solution (Fig. S1†). UV-vis spectroscopy measurements (Fig. S2†) are also in agreement with ESI-MS: the absorption profile of the as-prepared precursor solution matched closely with that of the $[HFe_3(CO)_{11}]^-$ cluster anion isolated using high performance liquid chromatography (HPLC).

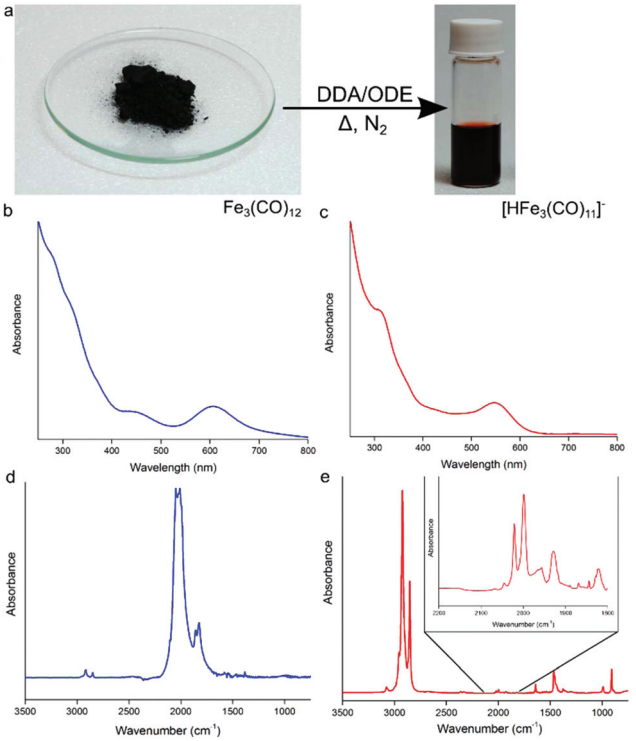

Fig. 1 (a) Schematic representation of the conversion of dark-green $Fe_3(CO)_{12}$, upon heating in an excess of 1-dodecylamine (DDA) in 1-octadecene (ODE) under an inert atmosphere, into dark-red $[HFe_3(CO)_{11}]^-$ anion that is fully soluble in the DDA/ODE mixture. (b) UV-Vis spectra of $Fe_3(CO)_{12}$ dissolved in $CHCl_3$. (c) UV-Vis spectrum of $[HFe_3(CO)_{11}]^-$ in ODE/DDA mixture (d) FTIR spectrum of $Fe_3(CO)_{12}$ in a KBr pellet. (e) FTIR spectrum of the as-formed $[HFe_3(CO)_{11}]^-$ cluster in a DDA/ODE mixture.

Results of FTIR spectroscopy are also consistent with the formation of the protonated iron carbonyl cluster anion. Fig. 1d shows the FTIR absorption spectrum of pure solid $Fe_3(CO)_{12}$ in the CO ligand stretching vibrations region that consists of two strong bands at 2050 cm^{-1} and 2010 cm^{-1} and weaker ones at 1860 cm^{-1} and 1825 cm^{-1}.[16] Fig. 1e shows the FTIR absorption spectrum of the $[HFe_3(CO)_{11}]^-$ anion in ODE/DDA solution. Present is a strong absorption band at ~2800 cm^{-1} corresponding to C–H stretches of excess DDA. The continued presence of terminal and bridging CO stretches (see Fig. 1e inset) points to the multi-metal iron center of the anionic cluster being maintained and is consistent with the formation of $[HFe_3(CO)_{11}]^-$.[13c,15b]

Once prepared, the precursor solution with $[HFe_3(CO)_{11}]^-$ is diluted in ODE and used as the iron source for nanoparticle synthesis, with the results shown in Fig. 2. The synthesis occurred at 200 °C under an inert atmosphere ensuring the

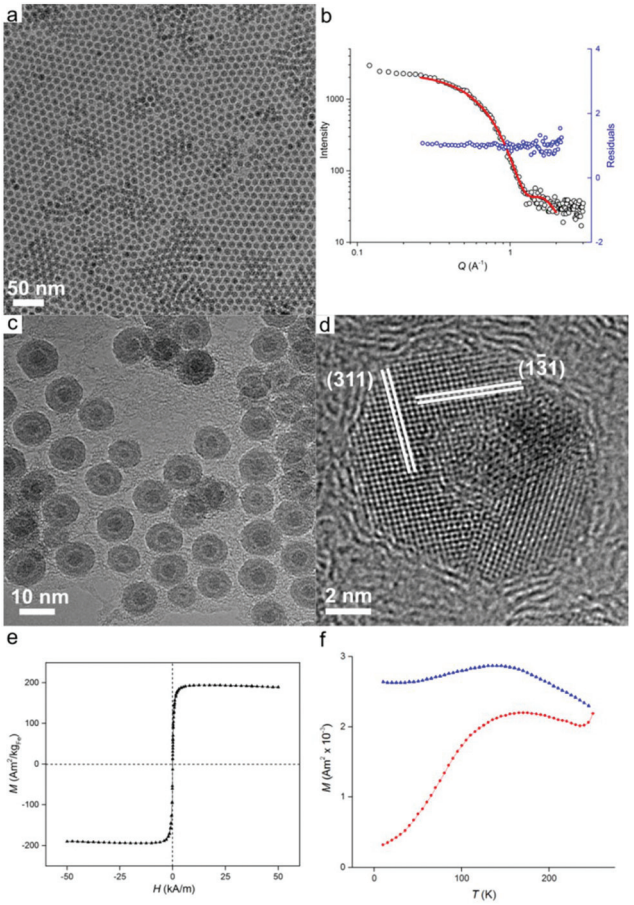

Fig. 2 (a) Transmission electron microscopy (TEM) image of Fe nanoparticles synthesized from the $[HFe_3(CO)_{11}]^-$ complex-containing precursor solution. (b) Small Angle X-ray Scattering (SAXS) data of Fe nanoparticles showing the raw data (black circles) overlaid with the model fit (red line) and residuals (blue circles). (c, d) HRTEM images of synthesized iron nanoparticles in lower (c) and higher (d) magnifications. Magnetite formation on the surface of Fe nanoparticles occurs during sample preparation. (e, f) Results of SQUID measurements on Fe nanoparticles. (e) Plot of magnetization (*M*) *vs.* applied field (*H*) showing the saturation magnetization. (f) Field cooled–zero field cooled (FC–ZFC) measurements establish the blocking temperature of 169 K, which indicates superparamagnetic behavior at room temperature.

formation of zero-valent iron. However, partial oxidation of particles during sample preparation for size analysis was observed leading to Fe/Fe_3O_4 core–shell nanoparticles (*vide infra*). Transmission electron microscopy (TEM) imaging (Fig. 2a) reveals well-dispersed particles of 9.3 ± 0.9 nm in diameter with regions of hexagonal and bilayer packing. The raw scattering data of a Small Angle X-ray scattering (SAXS) measurement together with a model curve and residuals are displayed in Fig. 2b. A spherical particle model with Gaussian size distribution (as observed from TEM) was used in the analysis of the scattering curves, giving an average nanoparticle size of 9.5 nm ± 1.0 nm, which is in good agreement with TEM results. We then show that good nanoparticle size control could be obtained. By varying the reaction temperature, oxidized iron nanoparticles of 11.1 ± 2.0 nm and 7.2 ± 0.7 nm in diameter could be formed at 180 °C and 280 °C, respectively (Fig. S3†).

Morphology of the oxidized iron nanoparticles is more clearly identifiable using high resolution TEM (Fig. 2c). The contrast difference between the oxide shell and the metal nanoparticle core is evident, together with a thin hollow interlayer produced by the Kirkendall effect during oxidation.[17]

No further growth of the hollow layer was observed under the electron beam. To calculate the size of the original nanoparticles that are present as zero-valent iron in solution (*i.e.*, before oxidation), the thickness of the oxide layer must be taken into account. Analysis of lattice planes (Fig. 2d) indicates the oxide shell could be indexed to polycrystalline magnetite Fe_3O_4,[18] which was further confirmed by X-ray diffraction analysis (Fig. S4†). Neither HRTEM or XRD showed evidence of bcc Fe, revealing the amorphous state of the iron particle core, which is not unexpected for iron nanoparticles of this size.[1b] The average thickness of the oxide shell was measured to be 2.9 ± 0.3 nm. Therefore the size of original Fe(0) nanoparticles in solution can be calculated as 7.9 ± 0.7 nm when the expansion of iron upon oxidation is taken into account.[19]

To investigate the magnetic properties of the unoxidized nanoparticles, an aliquot of the nanoparticle solution was sealed under vacuum (with extra care being paid to avoid oxidation), and its magnetic response was elucidated by means of superconducting quantum interference device (SQUID) magnetometry. The nanoparticles possess a saturation magnetization of 195 $Am^2\ kg^{-1}$ at 250 K, which is close to the value for bulk iron (Fig. 2e).[20] The particles are superparamagnetic at room temperature with a blocking temperature, T_B, of 169 K obtained from temperature-dependent field cooled (FC), zero-field cooled (ZFC) measurements (Fig. 2f). Superparamagnetism was also confirmed by the absence of noticeable remanence in Fig. 2e. The measured blocking temperature of these particles is much higher than what was expected for 7.9 nm bcc Fe nanoparticles.[5b] This has been previously observed for amorphous iron nanoparticles in this size range which indicates a significantly higher value of magnetocrystalline anisotropy, *K*.[1b,5b]

Besides the synthesis of homometallic Fe nanoparticles, the solution with $[HFe_3(CO)_{11}]^-$ anion can also be used in the synthesis of heterometallic particles: $Fe_{1-x}Co_x$ and $Fe_{1-x}Pt_x$. $Fe_{1-x}Co_x$ nanoparticles were synthesized from the thermal decomposition of a mixture of $[HFe_3(CO)_{11}]^-$ and $Co_2(CO)_8$ in ODE, with typical TEM images of the particles shown in Fig. 3. The particles were measured to be 9.4 ± 1.3 nm and 10.0 nm ± 1.4 nm in size, by TEM and SAXS, respectively (Fig. 3a and b). Results of the energy dispersive X-ray (EDX) spectroscopy are shown in Fig. 3c. After deconvolution of the overlapping CoK_α and FeK_β peaks (see inset), a quantitative analysis could be carried out using the Cliff–Lorimer equation.[21] The Cliff–Lorimer *k* factor, which is dimensionless and dependent on the TEM/EDX system used, was experimentally derived to be 0.96. We could then calculate an elemental composition of $Fe_{67}Co_{33}$ which is within the range known to display maximum magnetic saturation ($0.3 < x < 0.4$).[22] As prepared,

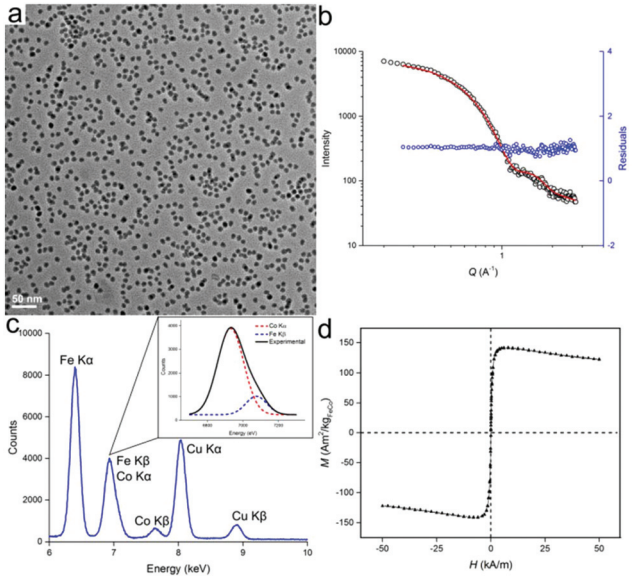

Fig. 3 $Fe_{1-x}Co_x$ nanoparticles from $[HFe_3(CO)_{11}]^-$ complex-containing precursor solution. (a) TEM image and (b) corresponding SAXS curves. (c) Energy dispersive X-ray (EDX) analysis along with deconvolution of overlapping CoK_α and FeK_β peaks (inset) allowing for quantitative analysis of both Fe and Co. (d) SQUID magnetic measurements of FeCo nanoparticles showing magnetization (*M*) *vs.* applied field (*H*).

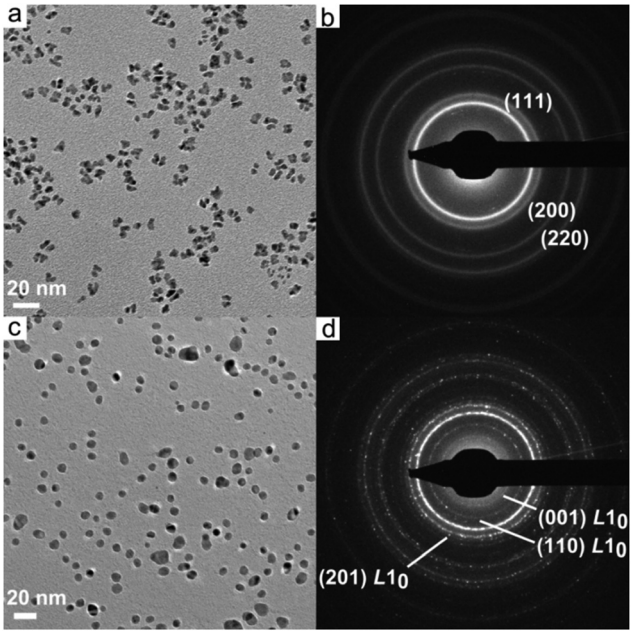

Fig. 4 $Fe_{1-x}Pt_x$ nanoparticles synthesized from the $[HFe_3(CO)_{11}]^-$ complex-containing precursor solution. TEM images of $Fe_{1-x}Pt_x$ particles (a) before and (c) thermal annealing at 750 °C for 30 min together with corresponding SAEDs (b and d) which can be indexed to the fcc crystal structure. SAED before annealing can be indexed to the fcc crystal structure, whereas after annealing SAED corresponds to the tetragonal $L1_0$ phase of $Fe_{1-x}Pt_x$.

$Fe_{67}Co_{33}$ nanoparticles were measured by SQUID to possess a magnetization of M_s = 142 Am^2 kg^{-1} at 250 K, which is comparable to previous examples of $Fe_{1-x}Co_x$ nanoparticles (Fig. 3d).[3d,23]

Fig. 4a shows a typical TEM image of $Fe_{1-x}Pt_x$ nanoparticles synthesized from a mixture of $[HFe_3(CO)_{11}]^-$ and $Pt(acac)_2$ prepared in dibenzyl ether (DBE). The nanoparticles have a branched morphology and are 7.7 ± 1.6 nm in size measured along the longest axis. EDX elemental analysis (Fig. S5, Table S2†) established the nanoparticle composition as $Fe_{50}Pt_{50}$. Selected area electron diffraction (SAED) pattern is given in Fig. 4b, which can be indexed to the face-centered cubic (fcc) crystal structure.[24] It is well-established that FePt particles must be thermally annealed to obtain the magnetically hard tetragonal $L1_0$ phase.[25] Therefore, the as-synthesized nanoparticles were annealed *in situ* at 750 °C for 30 min using a TEM heating stage, with the results shown in Fig. 4c. The shape of the particles becomes more rounded due to the minimization of their surface area, with the average size being slightly reduced to 7.2 ± 1.1 nm. A SAED pattern (Fig. 4d) shows the emergence of the (001), (110) and (201) reflections of the tetragonal $L1_0$ phase. HRTEM experiments were also performed, confirming the transformation to the tetragonal phase upon annealing (Fig. S6†). Particle coalescence is avoided by annealing directly on the TEM substrate.

Similarly to $Fe_3(CO)_{12}$, the non-volatile diiron carbonyl cluster $Fe_2(CO)_9$ is also known to react with strong bases, including amines.[15] The possibility of using $Fe_2(CO)_9$ to form the $[HFe_3(CO)_{11}]^-$ anionic cluster in solution was also investigated. The $Fe_2(CO)_9$ cluster readily dissolves in a DDA/ODE mixture upon heating forming an orange-red solution (see FTIR analysis, Fig. S7†). The thermal decomposition of this precursor solution also yields metallic iron, $Fe_{1-x}Co_x$, and $Fe_{1-x}Pt_x$ nanoparticles, similar to those obtained from the $Fe_3(CO)_{12}$ case. To the best of our knowledge, prior to this work, only Kramer *et al.* used $Fe_2(CO)_9$ dissolved in ionic liquids to obtain Fe and Fe_2O_3 nanoparticles. However, only small particles were formed (~4 nm) and they subsequently readily agglomerated.[26] Here, the oxidized iron nanoparticles were measured to be 10.8 ± 0.9 nm and 10.2 nm ± 1.3 nm, by TEM and SAXS, respectively (Fig. S8 and 9†). The size of $Fe_{1-x}Co_x$ alloy nanoparticles was found to be 9.6 ± 1.6 nm and 10.3 nm ± 1.6 nm, by TEM and SAXS, respectively (Fig. S10a and b†). From EDX analysis, they were shown to possess $Fe_{55}Co_{45}$ composition (Fig. S10c and d†). The $Fe_{1-x}Pt_x$ nanoparticles were 7.4 ± 0.5 nm in size (from SAXS analysis) and had a composition of $Fe_{35}Pt_{65}$, which is within the requirements for tetragonal ordering (Fig. S11 and 12, Table S3†).[27] The size and composition of pure iron and iron-containing heterometallic nanoparticles obtained from $Fe_2(CO)_9$ were similar to that formed using $Fe_3(CO)_{12}$ indicating the versatility of our approach for the solubilization of multi-nuclear iron carbonyl clusters. The lighter color of the final reaction solution formed with $Fe_2(CO)_9$ indicates a lower concentration of $[HFe_3(CO)_{11}]^-$ (Fig. S7†). This explains the subtle variations in reaction temperatures required for the formation of well-defined nanoparticles (see Experimental section). This change

in reaction kinetics with $[HFe_3(CO)_{11}]^-$ concentration also indicates that it is the major species responsible for nanoparticle formation. While the solutions formed from both iron carbonyl compounds used here are not simple stoichiometric compounds, this study supports our previous observation that non-stoichiometric precursors can produce extremely reproducible results, if consistently prepared.[15c]

Conclusions

In summary, we have demonstrated that by the straightforward mixing of insoluble iron carbonyls $Fe_3(CO)_{12}$ or $Fe_2(CO)_9$ with an amine surfactant, a precursor solution containing the $[HFe_3(CO)_{11}]^-$ anionic cluster can be formed. This solution, in turn, can be used as a direct replacement for iron pentacarbonyl in a variety of nanoparticle forming reactions, including the thermolytic synthesis of Fe, $Fe_{1-x}Co_x$, and $Fe_{1-x}Pt_x$ nanoparticles. Compared to more commonly used techniques, the use of solutions of these non-volatile cluster solutions as iron precursors allow for safer reactions and improved synthetic control for the formation of iron and iron-containing heterometallic nanoparticles.

Acknowledgements

Supported by the Laboratory Directed Research and Development program at Sandia National Laboratories. This work was performed, in part, at the Center for Integrated Nanotechnologies, an Office of Science User Facility operated for the U.S. Department of Energy (DOE) Office of Science. Sandia National Laboratories is a multi-program laboratory managed and operated by Sandia Corporation, a wholly owned subsidiary of Lockheed Martin Corporation, for the U.S. Department of Energy's National Nuclear Security Administration under contract DE-AC04-94AL85000. Los Alamos National Laboratory, an affirmative action equal opportunity employer, is operated by Los Alamos National Security, LLC, for the National Nuclear Security Administration of the U.S. Department of Energy under contract DE-AC52-06NA25396.

Notes and references

1 (*a*) D. L. Huber, *Small*, 2005, **1**, 482–501; (*b*) T. C. Monson, Q. Ma, T. E. Stevens, J. M. Lavin, J. L. Leger, P. V. Klimov and D. L. Huber, *Part. Part. Syst. Charact.*, 2013, **30**, 258–265; (*c*) L. M. Lacroix, N. F. Huls, D. Ho, X. L. Sun, K. Cheng and S. H. Sun, *Nano Lett.*, 2011, **11**, 1641–1645; (*d*) A. H. Lu, E. L. Salabas and F. Schüth, *Angew. Chem., Int. Ed.*, 2007, **46**, 1222–1244; (*e*) C. J. Meledandri and D. F. Brougham, *Anal. Methods*, 2012, **4**, 331–341.

2 (*a*) D. A. J. Herman, P. Ferguson, S. Cheong, I. F. Hermans, B. J. Ruck, K. M. Allan, S. Prabakar, J. L. Spencer, C. D. Lendrum and R. D. Tilley, *Chem. Commun.*, 2011, **47**, 9221–9223; (*b*) S. Cheong, P. Ferguson, I. F. Hermans, G. N. L. Jameson, S. Prabakar, D. A. J. Herman and R. D. Tilley, *ChemPlusChem*, 2012, **77**, 135–140; (*c*) A. B. Salunkhe, V. M. Khot and S. H. Pawar, *Curr. Top. Med. Chem.*, 2014, **14**, 572–594; (*d*) T. A. P. Rocha-Santos, *Trends Anal. Chem.*, 2014, **62**, 28–36; (*e*) Y.-W. Jun, J.-H. Lee and J. Cheon, *Angew. Chem., Int. Ed.*, 2008, **47**, 5122–5135; (*f*) R. Hudson, A. Riviere, C. M. Cirtiu, K. L. Luska and A. Moores, *Chem. Commun.*, 2012, **48**, 3360–3362.

3 (*a*) C. Desvaux, F. Dumestre, C. Amiens, M. Respaud, P. Lecante, E. Snoeck, P. Fejes, P. Renaud and B. Chaudret, *J. Mater. Chem.*, 2009, **19**, 3268–3275; (*b*) C. Desvaux, C. Amiens, P. Fejes, P. Renaud, M. Respaud, P. Lecante, E. Snoeck and B. Chaudret, *Nat. Mater.*, 2005, **4**, 750–753; (*c*) X. B. Su, H. G. Zheng, Z. P. Yang, Y. C. Zhu and A. L. Pan, *J. Mater. Sci.*, 2003, **38**, 4581–4585; (*d*) G. S. Chaubey, C. Barcena, N. Poudyal, C. Rong, J. Gao, S. Sun and J. P. Liu, *J. Am. Chem. Soc.*, 2007, **129**, 7214–7215.

4 (*a*) S. H. Sun, C. B. Murray, D. Weller, L. Folks and A. Moser, *Science*, 2000, **287**, 1989–1992; (*b*) K. Elkins, D. Li, N. Poudyal, V. Nandwana, Z. Q. Jin, K. H. Chen and J. P. Liu, *J. Phys. D: Appl. Phys.*, 2005, **38**, 2306–2309; (*c*) S. H. Sun, *Adv. Mater.*, 2006, **18**, 393–403.

5 (*a*) S. Cheong, P. Ferguson, K. W. Feindel, I. F. Hermans, P. T. Callaghan, C. Meyer, A. Slocombe, C.-H. Su, F.-Y. Cheng, C.-S. Yeh, B. Ingham, M. F. Toney and R. D. Tilley, *Angew. Chem., Int Ed.*, 2011, **50**, 4206–4209; (*b*) T. C. Monson, E. L. Venturini, V. Petkov, Y. Ren, J. M. Lavin and D. L. Huber, *J. Magn. Magn. Mater.*, 2013, **331**, 156–161; (*c*) Y. P. Sun, X. Q. Li, J. S. Cao, W. X. Zhang and H. P. Wang, *Adv. Colloid Interface Sci.*, 2006, **120**, 47–56; (*d*) D. A. J. Herman, S. Cheong-Tilley, A. J. McGrath, B. F. P. McVey, M. Lein and R. D. Tilley, *Nanoscale*, 2015, **7**, 5951–5954; (*e*) B. Bian, W. Xia, J. Du, J. Zhang, J. P. Liu, Z. Guo and A. Yan, *Nanoscale*, 2013, **5**, 2454–2459.

6 Occupational Safety and Health Administration [OSHA], Retrieved from; https://www.osha.gov/dts/chemicalsampling/data/CH_247500.html.

7 H. G. Cutforth and P. W. Selwood, *J. Am. Chem. Soc.*, 1943, **65**, 2414–2415.

8 N. Shpaisman, E. R. Bauminger and S. Margel, *J. Alloys Compd.*, 2008, **454**, 89–96.

9 M. Kin, H. Kura, M. Tanaka, Y. Hayashi, J. Hasaegawa and T. Ogawa, *J. Appl. Phys.*, 2015, **117**, 17E714.

10 (*a*) R. B. King and F. G. A. Stone, *J. Am. Chem. Soc.*, 1960, **82**, 4557–4562; (*b*) H. Yamada, S. Aoyagi and C. Kibayashi, *J. Am. Chem. Soc.*, 1996, **118**, 1054–1059; (*c*) S. Enthaler, M. Haberberger and E. Irran, *Chem. – Asian J.*, 2011, **6**, 1613–1623; (*d*) G. K. Jarugumilli and S. P. Cook, *Org. Lett.*, 2011, **13**, 1904–1907.

11 D. Amara, I. Felner, I. Nowik and S. Margel, *Colloids Surf., A*, 2009, **339**, 106–110.

12 A. Choplin, L. Huang, A. Theolier, P. Gallezot, J. M. Basset, U. Siriwardane, S. G. Shore and R. Mathieu, *J. Am. Chem. Soc.*, 1986, **108**, 4224–4225.

13 (*a*) W. Hieber and R. Werner, *Chem. Ber.*, 1957, **90**, 1116–1120; (*b*) W. F. Edgell, M. T. Yang, B. J. Bulkin, R. Bayer and N. Koizumi, *J. Am. Chem. Soc.*, 1965, **87**, 3080–3088; (*c*) F. Hugues, J. M. Bassett, Y. B. Taarit, A. Choplin, M. Primet, D. Rojas and A. K. Smith, *J. Am. Chem. Soc.*, 1982, **104**, 7020–7024.

14 D. Zitoun, C. Amiens, B. Chaudret, M. C. Fromen, P. Lecante, M. J. Casanove and M. Respaud, *J. Phys. Chem. B*, 2003, **107**, 6997–7005.

15 (*a*) W. Hieber and H. Beutner, *Z. Naturforsch., B: Anorg. Chem. Org. Chem. Biochem. Biophys. Biol.*, 1962, **17**, 211–&; (*b*) F. Hugues, A. K. Smith, Y. B. Taarit, J. M. Basset, D. Commereuc and Y. Chauvin, *J. Chem. Soc., Chem. Commun.*, 1980, 68–70; (*c*) H. Kuroda, *Pure Appl. Chem.*, 1992, **64**, 1449–1460.

16 (*a*) R. K. Sheline, *J. Am. Chem. Soc.*, 1951, **73**, 1615–1618; (*b*) F. A. Cotton and G. Wilkinson, *J. Am. Chem. Soc.*, 1957, **79**, 752–753.

17 (*a*) D. A. J. Herman, S. Cheong, M. J. Banholzer and R. D. Tilley, *Chem. Commun.*, 2013, **49**, 6203–6205; (*b*) Y. D. Yin, R. M. Rioux, C. K. Erdonmez, S. Hughes, G. A. Somorjai and A. P. Alivisatos, *Science*, 2004, **304**, 711–714.

18 Magnetite is indistinguishable from another iron oxide, maghemite (Fe_2O_3), with the characterization tools employed here. However for our purposes, the assumption of a magnetite phase is sufficient.

19 Y. Zhao, H. Ren, H. Dai and W. Jin, *Corros. Sci.*, 2011, **53**, 1646–1658.

20 B. D. Cullity, *Introduction to Magnetic Materials*, Addison-Wesley Publishing Company, Reading, 1972.

21 D. B. Williams and C.B. Carter, *Transmission Electron Microscopy: IV Spectrometry*, Springer Science, 1996.

22 (*a*) Y. Fu, X. F. Cheng and Z. Yang, *Phys. Status Solidi A*, 2006, **203**, 963–969; (*b*) P. Sirvent, E. Berganza, A. M. Aragón, A. Bollero, A. Moure, M. García-Hernández, P. Marín, J. F. Fernández and A. Quesada, *J. Appl. Phys.*, 2014, **115**, 17B505; (*c*) S. Farabi Khaneghahi and S. Sharafi, *Adv. Powder Technol.*, 2014, **25**, 211–218.

23 (*a*) V. Tzitzios, G. Basina, D. Niarchos, W. Li and G. Hadjipanayis, *J. Appl. Phys.*, 2011, **109**, 07A313; (*b*) C. Desvaux, P. Lecante, M. Respaud and B. Chaudret, *J. Mater. Chem.*, 2010, **20**, 103–109.

24 W. Lv, W. He, X. Wang, Y. Niu, H. Cao, J. H. Dickerson and Z. Wang, *Nanoscale*, 2014, **6**, 2531–2547.

25 (*a*) D. R. Li, N. Poudyal, V. Nandwana, Z. Q. Jin, K. Elkins and J. P. Liu, *J. Appl. Phys.*, 2006, **99**; (*b*) A. Delattre, S. Pouget, J. F. Jacquot, Y. Samson and P. Reiss, *Small*, 2010, **6**, 932–936.

26 J. Krämer, E. Redel, R. Thomann and C. Janiak, *Organometallics*, 2008, **27**, 1976–1978.

27 M. Delalande, M. J. F. Guinel, L. F. Allard, A. Delattre, R. Le Bris, Y. Samson, P. Bayle-Guillemaud and P. Reiss, *J. Phys. Chem. C*, 2012, **116**, 6866–6872.